Optogenetic-Induced Muscle Loading Leads to Mechanical Adaptation of the Achilles Tendon Enthesis in Mice

Elahe Ganji[1,2,3*]

Syeda N. Lamia[1,4*]

Matthew Stepanovich[1]

Noelle Whyte[1]

Robert W. Goulet[1]

Adam C. Abraham[1]

Megan L. Killian[1,3]

1. Department of Orthopaedic Surgery, Michigan Medicine, University of Michigan, 109 Zina Pitcher Pl., Ann Arbor, Michigan, 48109
2. Beckman Institute for Advanced Science and Technology, University of Illinois at Urbana-Champaign, 405 North Mathews Ave., Urbana, Illinois, 61801
3. Department of Biomedical Engineering, University of Delaware, 540 S. College Ave., Newark, Delaware, 19713
4. Department of Mechanical Engineering, University of Michigan, 2350 Hayward St., Ann Arbor, Michigan, 48109

*equal contributions

Address for Correspondence:

Megan Killian

Assistant Professor of Orthopaedic Surgery

Michigan Medicine

University of Michigan

109 Zina Pitcher Pl.

BSRB 2021

Ann Arbor, MI 48109

mlkillia@med.umich.edu

Keywords: enthesis, optogenetics, musculoskeletal growth, 3D imaging, mechanobiology, tendon, bone, RNA sequencing

Short title: Light-activated muscle loading of tendon and bone

Abstract

Skeletal shape depends on transmission of contractile muscle forces from tendon to bone across the enthesis. Loss of muscle loading impairs enthesis development, yet little is known if and how the postnatal enthesis adapts to increased loading. Here, we studied adaptations in enthesis structure and function in response to increased loading using optogenetically-induced muscle contraction in young (i.e., growth) and adult (i.e., mature) mice. Daily bouts of unilateral optogenetic loading in young mice led to radial calcaneal expansion and warping. This also led to a weaker enthesis with increased collagen damage, with little change in adult mice. We then used RNA-sequencing to identify pathways associated with increased mechanical loading during growth. In tendon, we found enrichment of glycolysis, focal adhesion, and cell-matrix interactions. In bone, we found enrichment of inflammation and cell cycle. Together, we demonstrate the utility of optogenetic-induced muscle contraction to elicit in vivo adaptation of the enthesis.

Introduction

The enthesis is a tissue interface that adapts to applied muscle loads during postnatal growth by forming a graded fibrocartilage transition between tendon and bone (*1–4*). The mature enthesis is a network of mineralized and unmineralized collagen fibers that is tougher than either tendon or bone (*5*). As the result of this structural toughening, acute and high energy-induced tendon injuries typically result in failure of tendon (e.g., Achilles tendon ruptures) or bone (e.g., calcaneal avulsion fractures) and not the enthesis (*6*). However, with chronic and repetitive loading, the enthesis is susceptible to localized damage and overuse-related injuries, and up to 25% of all chronic tendon and ligament disorders involve the enthesis (*7–10*). In fact, overuse is considered the underlying cause of most entheseal disorders (e.g., Achilles insertional tendinopathy, Sever disease) that are most commonly observed in young athletes (*7*, *11*, *12*). For example, Sever disease, classified as pain adjacent to the Achilles enthesis, is considered an inflammatory condition of the calcaneal apophysis caused by high levels of physical activities in children (*13*). However, there does exist uncertainty related to this diagnosis with a lack of clear evidence regarding its pathophysiology.

Yet loading is essential for functional development and growth of the tendon-bone enthesis (*9*, *14–16*). During embryonic development, tendon extends from the cartilage anlagen to guide load transfer from skeletal muscle which induces the mechano-adaptive growth of the enthesis (*17*). During postnatal development, the enthesis matures into a graded fibrocartilage interface from the fibrous tendon to the mineralized bone (*9*, *14*). The structural adaptation of the enthesis occurs in response to a combination of tensile and compressive loads (*4*, *9*, *18*). While several elegant studies have established the requirement of muscle contraction during musculoskeletal growth, these studies have primarily focused on the absence or reduction of muscle loading rather than increased muscle contraction (*17*, *19*, *20*). Yet increased activity during periods of rapid growth, such as in children and during adolescence, can lead to micromotion at the enthesis and apophysis and result in pain and clinical presentation of disorders such as Sever disease (*7*, *8*). In adults, repeated tendon loading during activities like running-associated overuse can lead to abnormalities such as bony spur formation at the distal tendon that leave individuals with pain and dysfunction (*2*, *9*). Despite the potential age-associated differences in adaptation of the enthesis to repeated loading, the mechanisms contributing to enthesis adaptation of the immature and mature skeleton remain poorly understood and challenging to study (*21*).

In mouse and rat studies of skeletal adaptation to mechanical loading, cyclic, sub-failure compressive loading has commonly been used to induce anabolic bone formation in both the ulna and tibia (*22–26*). Similarly, sub-failure cyclic tensile loading of the patellar tendon has been used to model tendon fatigue and damage in mice and rats (*27*, *28*). Unfortunately, the latter approach does not load tendon enthesis via muscle contraction but instead via direct, open, and external mechanical actuation. More commonly used and physiologically-relevant models of tendon loading, such as forced treadmill running (uphill or downhill), are effective for inducing structural changes to the mature enthesis in response to increased loading but also have their drawbacks (*29–32*). For example, treadmill running studies in mice and rats, like most bone anabolic loading studies, typically initiate forced running at 7-8 weeks of age (*33*), which limits our ability to study tendon and enthesis adaptation during maturation. Additionally, these approaches are highly variable, as even inbred mouse strains have high variations in distances run and tolerance for forced treadmill running (*34*). Forced treadmill running can also confound results by inducing anxiety, leading to systemic inflammation (*35*) as well as effect organismal metabolic conditioning induced by cardiovascular load and training effects (*36*). To counter the systemic effects and reduce loading dose variability, electrical nerve stimulation has also been used to induce repeated muscle stimulation in mice and rats for tendon loading (*37*, *38*). However, this approach is also challenging, as most studies are in adult animals and these approaches require subdermal needle electrode placement which may increase risk of injury and infection with repeated electrode placement in the growing muscle and tendon. Thus, understanding how loading effects structural changes to the tendon enthesis during growth has been challenging *in vivo* because of a lack of physiologically relevant loading models.

To address these challenges, we turned to the use of optogenetics as a non-invasive tool for direct and precise induction of muscle contraction for *in vivo* tendon loading in growing mice. Optogenetics is a tool commonly used in neuroscience that facilitates controlled activation of activatable cells such as neurons and muscle cells, with high spatial and temporal specificity (*39*). Channelrhodopsin-2 (ChR2) is a light-sensitive microbial opsin that, when present on the cell membrane, acts as a non-specific light-activated cation channel that induces membrane depolarization (*40*, *41*). Optogenetic stimulation improves the spatial specificity of electrical stimulation by targeting cell subpopulations based on morphological markers and molecular footprint (*42*). We and others have previously shown that optogenetic-mediated activation of

skeletal muscle allows for precise and controlled contraction of specific muscle groups (*43–45*) and, therefore, their associated tendons and entheses. In this study, we used pulsatile transcutaneous exposure of ChR2 expressing skeletal muscle cells to collimated blue LED light (455 nm) to induce isometric activation of triceps surae muscles. We examined how sustained daily bouts of optogenetic activation can differentially elicit structural, functional, and molecular changes in the young and adult Achilles enthesis of mice. We then defined transcriptional changes in the Young tendon and bone following repeated loading.

Results

Optogenetic activation is a repeatable and safe approach for daily tendon loading

To investigate the effects of increased loading on the postnatal Achilles enthesis, we generated a transgenic mouse line to express ChR2 in skeletal muscle (doxycycline-treated Ai32-floxed, ACTA1-rtTA;tetO-Cre mice (*44*) and unilaterally loaded their Achilles tendon using optogenetic stimulation of the triceps surae muscle. Daily bouts of loading were delivered under isoflurane anesthesia at either 5- or 20-minute bouts for 5 days a week, up to 3 weeks (19 days) in duration, in mice starting at either 4 weeks of age (Young group; this time point coincides with enthesis growth) or at 6-8 months of age (Adult group, 20-min bouts only; mature enthesis). In Young mice, the steady state generated torque at the end of the 20-minute loading bout was ~30% of the initial peak torque for the first week of daily optogenetic muscle loading. We found that daily loading in Young mice did not negatively impact animal weight gain, however some weight loss was observed in Adult mice (Fig. 1A). Isometric ankle joint torque did not significantly vary over the course of the experiment for the Young group but did increase with daily 20-minute loading bouts in the Adult group from week 1 to week 2 of loading (Fig. 1B). A subset of mice were used to measure ankle torque for the first five consecutive days and throughout the duration of loading. Peak torque (~3N-mm), generated by the hindlimb muscles in Young mice, was measured in the first 1-2 cycles of loading (cycle = 70ms light on, 30ms light off; every 5 seconds) and steady state torque (~1N-mm) was generated around 500-750 cycles (~100-125 cycles) (Fig. 1C). To test the response to optogenetic stimulation in adult mice, we isolated the extensor digitorum longus (EDL) muscle from an adult (3-month-old) mouse treated with doxycycline during gestation and up to weaning (21 days of age) and measured twitch forces *in vitro* in response to blue light exposure. We were able to elicit strong and duration-dependent force generation, which indicates sufficient ActaCre-ChR2 recombination (Fig. 1D).

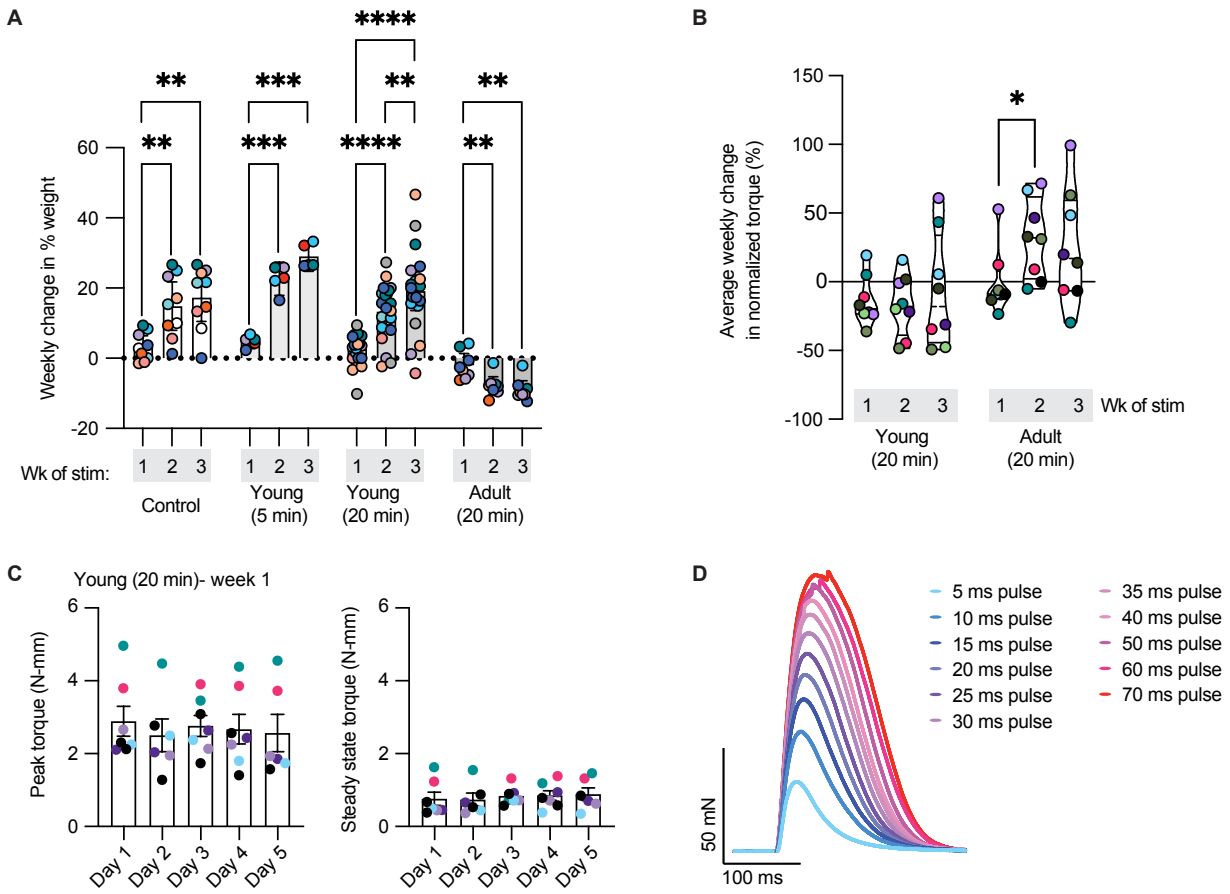

Fig. 1. Optogenetic activation of triceps surae muscle group is not invasive and does not negatively influence animal weight or generated isometric ankle joint torque in Young mice. (A) Young mice, regardless of exposure to daily bouts of optogenetic muscle stimulation (5- or 20-minute duration), gained weight for the duration of the experiment. However, adult mice lost weight (~10%) from onset to end of the experiment. Control were naïve mice at similar ages as the Young group. (B) Normalized torque significantly increased in adult but not young mice with daily bouts of 20-minute optogenetic muscle stimulation. Each data point denotes average weekly change in generated ankle torque normalized to weight of the animal. (C) The steady state generated ankle torque (at the end of the 20-minute loading bout), measured during isometric ankle plantarflexion, was ~30% of the peak torque in young mice for the first week of daily optogenetic muscle loading. (D) EDL muscle from an adult (3month old) ActaCre;Ai32 mouse had a duration-dependent force response to blue light exposure measure contraction when tested *in vitro* (5ms-70ms). For panels A and B, data were compared using two-way ANOVA with mixed models (repeated measures between weeks within groups, Sidak correction). Error bars: *Mean ± 95% confidence interval.* *: $p < 0.05$, **: $p < 0.001$, ****: $p < 0.0001$, and ***: $p = 0.0004$.

Daily tendon loading leads to bony changes and impaired mechanical properties of the Young but not Adult Achilles enthesis

Daily loading of the tendon and enthesis for 3 weeks (19 days) led to apophyseal shape changes in the Young calcanei (Fig. 2A). Quantitative differences in the shape of the Young calcaneus in response to optogenetic-induced loading were measured as three major mode shape changes, such as shortening (Mode 1: 63.7% shape change; shown in blue in Fig. 2A on deformation maps in posterior view), expansion/breathing mode (Mode 2: explaining 13.3% shape change), and warping (Mode 3: highlighted in Fig. 2A; shown in red on deformation maps in both lateral and medial views). The adult calcaneus was not significantly different in length compared to control calcaneus, and we did not measure differences in volume or bone volume percentage (BV/TV) with loading compared to contralateral controls. However, the Young calcaneus was smaller in volume with loading and had increased BV/TV (Fig. 2B). Neither Young (Fig. 2B) or Adult exhibited significant change in length from the calcaneal tuberosity to the peroneal tubercle. With shorter loading bouts (i.e., 5 min loading duration), we did not observe any significant differences in Young calcaneal length, TV, or BV/TV compared to contralateral controls (Table S1).

All tissues failed at the enthesis (Young and Adult) or calcaneal growth plate (Young), not the tendon mid-substance, during uniaxial testing. In Young mice, the maximum load before failure was significantly reduced following repeated loading compared to contralateral Achilles tendon and enthesis (Fig. 2C). However, increased strength was observed in the Adult tendon/enthesis following 3 weeks of loading compared to the contralateral tendons (Fig. 2C). For the Young, but not Adult, Achilles tendon/enthesis, toughness was significantly reduced after 3 weeks of loading compared to contralateral tendons (Fig. 2C).

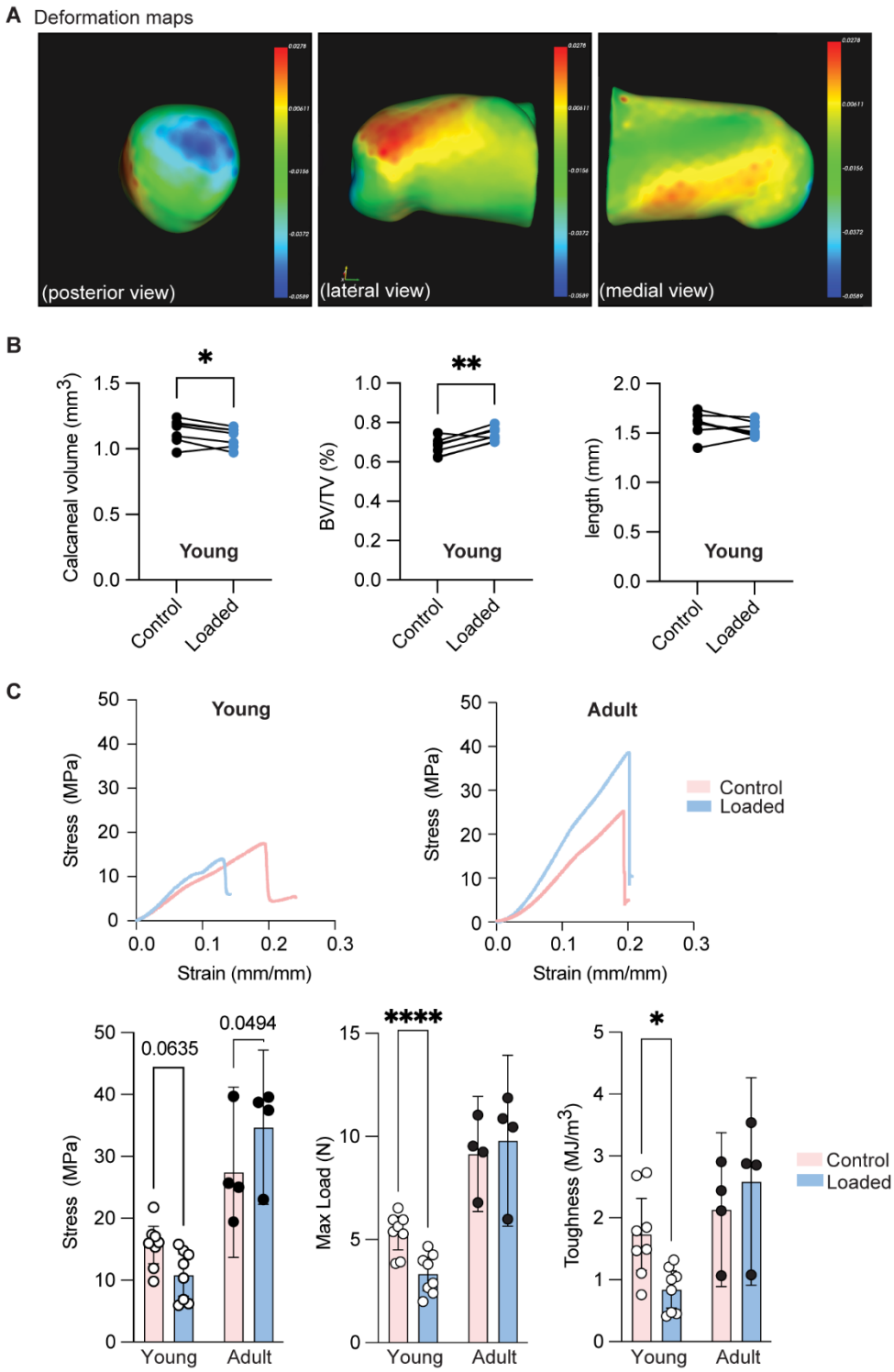

Fig. 2. Repeated daily loading of Young mouse Achilles tendons results in expansion and warping deformation and impaired mechanical toughness at the enthesis. (A) Deformation maps of the posterior, lateral, and medial views of loaded (average shape; right calcaneus) compared to control (average shape, left calcaneus, mirrored for overlay/shape representation) showed reduced height of the calcaneal tuberosity with loading (posterior view; shown in blue)

and increased bone expansion and warping (lateral and medial views; shown in red). (B) Total volume of the calcaneal region of interest was significantly reduced with loading (paired t-test; $p = 0.0338$), and bone volume percentage (BV/TV; %) was significantly increased (paired t-test; $p = 0.0056$) in Young loaded compared to Young control calcanei. No significant differences in length between Young control and loaded calcanei were measured. (C) Representative stress-strain curves for young and adult groups showed structural adaptations in the Young enthesis and apophysis coincide with significantly reduced tensile strength and toughness in the loaded compared to non-loaded contralateral limbs. Data were compared using two-way ANOVAs with multiple comparisons (contralateral vs. loaded; no correction for sphericity; Sidak correction for multiple comparisons). *Error bars: Mean ± 95% confidence interval*. *: $p< 0.05$, ****: $p < 0.0001$.

Daily tendon loading leads to accumulated collagen damage in Young mice

Loading can initiate accumulative damage at the molecular level by inducing fibril breaks and protease-induced remodeling of the extracellular matrix (ECM). As a result of this ECM damage, collagen triple helices can irreversibly unfold (*46*). To evaluate collagen damage in our *in vivo* model of tendon loading, we used collagen hybridizing peptides (CHPs) conjugated with fluorescent labels to visualize molecular-level damage *in vivo* (*47*, *48*). In tendon, CHPs can specifically detect non-recoverable (post-yield) unfolding of collagen fibers (*46*). After 5 consecutive days of 20-minute daily loading bouts, Young loaded tendon and enthesis had higher CHP intensity (Fig. 3B) and, therefore, collagen denaturation than contralateral controls ($p=0.0074$). Collagen type III is correlated with increased remodeling, however the ~~loaded~~ attachments did not have quantitatively more Collagen type III+ cells or aggrecan within the enthesis compared to controls (Fig. 3C, E) following 3 weeks (19 days) of loading. Histologically, we also observed thinning of the Young fibrocartilage enthesis and smaller, but not fewer, cells with loading (Fig. 3D, F). We did not observe any major morphological differences between loaded Young entheses with 5min daily loading bouts compared to 20min bouts (Fig. S1).

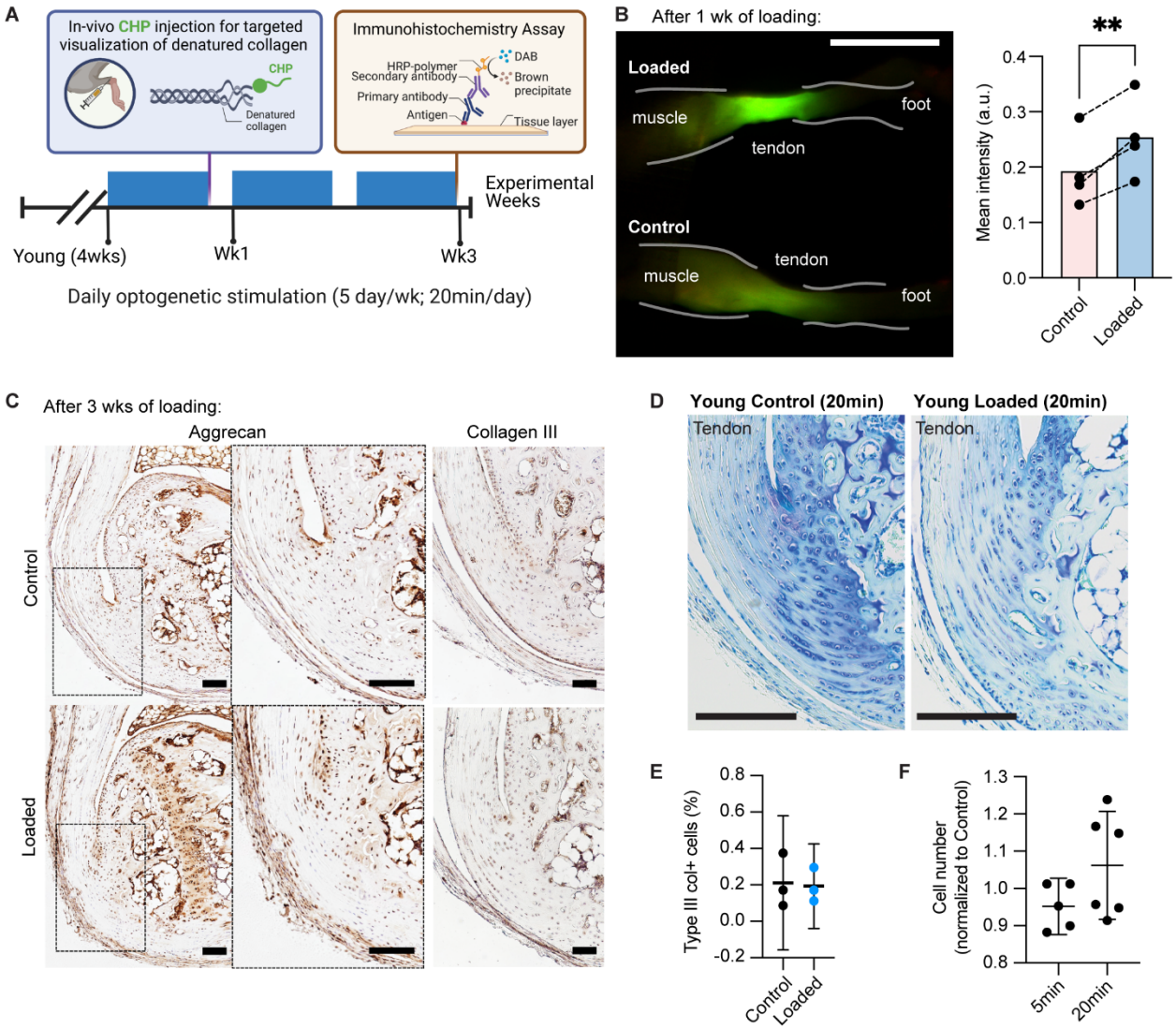

Fig. 3. Repeated loading led to denatured collagen fibers and increased prevalence of ECM components at the enthesis and growth plate. (A) Schematic shows experimental design for evaluation of effect of repeated loading on ECM of the Young tendon and enthesis. (B) Repeated loading resulted in the accumulation of collagen denaturation in loaded tendon and enthesis. Data compared using paired t-test (two-tailed; assuming Gaussian distribution, parametric; **: $p = 0.0062$. (C, E) Loaded entheses did not exhibit differences in localized Aggrecan or Type III Collagen at the enthesis compared to controls. Type III Collagen cell count data were compared using unpaired t-tests (non-parametric; Mann-Whitney test; two-tailed; $p > 0.9999$). (D) However, loading qualitatively influenced pericellular matrix and cell shape, but not cell number, at the enthesis in Young mice. (F) Cell number was not affected by duration of loading (5min vs. 20min; unpaired non-parametric t-test; Mann-Whitney, two-tailed; $p = 0.1342$). Scale bars: B, 10mm; C, D, 100 µm. *Error bars: Mean ± 95% confidence interval*.

Transcriptomics

We performed bulk RNA-seq with RNA isolated from Achilles tendons and calcanei of naïve and optogenetically-loaded Young mice (loaded and contralateral limbs) at 4 hr post-final loading bout to investigate the molecular changes underlying the structural enthesis and bone morphology. We used principal component analyses (PCA) to evaluate data quality in an unsupervised approach (Fig. 4A). To avoid any compensatory effects of the contralateral limb and because we saw discrete separation of naïve from loaded (5 day and 12 day) tendons in PCA, we used naïve data to measure fold change between optogenetically loaded and cage activity tendons and bones (Fig. 4A). We identified 1,193 and 312 genes in tendon and bone, respectively, that were differentially expressed at both 5 and 12 days of loading (Fig. 4B and C), and both tendon and bone had more differentially expressed genes at 12 days compared to 5 days of daily loading. A full list of differentially expressed genes (DEGs) is provided in the supplementary material S3.

We used The Database for Annotation, Visualization, and Integrated Discovery (DAVID) to further analyze biological processes and Kyoto Encyclopedia of Genes and Genomes (KEGG) pathways. We found several biological processes were enriched in both tendon and bone, including angiogenesis, extracellular matrix organization, cellular response to TGF-beta stimulus, and response to mechanical stimulus (Fig. 5). Additionally, in tendon, we found FGF receptor signaling was enriched after 5 days of loading, and canonical glycolysis was enriched after 12 days of loading (Fig. 5A). In bone, we found integrin-mediated signaling and inflammatory response were enriched after 12 days of loading and collagen fibril organization and DNA replication initiation was enriched after 12 days of loading (Fig. 5B).

We found optogenetic loading resulted in downregulation of numerous genes associated with tendon stem cells, including *Tppp3, Tnc,* and *Fbn1*, which were down at both 5 and 12 days, (Fig. 6). Of the top 20 downregulated genes (based on log2FC) in tendon following loading, most were associated with extracellular matrix synthesis at one or both time points, including *Matn3*, *Acan*, *Col8a1*, *Thbs1*, *Col9a2*, *Bglap*, *Mmp9*, *Col2a1*, and *Adamts19* (Fig. 6). This was further confirmed using KEGG pathway analysis in DAVID, in which focal adhesion, ECM-receptor interaction, and regulation of actin cytoskeleton were significantly enhanced at both 5 and 12 day time points (Fig. 7A). ECM-receptor interaction was significantly downregulated with loading in tendon at both 5 and 12 days compared to naïve control tendons (Fig. 7C). In bone, daily bouts of loading resulted in increased expression of *Il1ra2*, *Ccl21c*, *Ccl21a*, *Gpnmb*,

and *Ccl19* and other pro-inflammatory markers at one or both time points (Fig. 6). We also found that *Ihh* was one of the top 20 downregulated genes in bone at both 5 and 12 days with loading (Fig. 6). Activation of the KEGG pathway, focal adhesion, identified bout-dependent changes in gene expression, especially for *Tnc*, *Col1a1*, *Col1a2*, and *Thbs4* in bone (Fig. 7D). Expression of *Tnc*, as well as *Col1a1*, *Col1a2*, and *Col2a1*, were consistent in follow-up experiments using quantitative real-time reverse-transcription polymerase chain reaction (qRTPCR) on cDNA from tendon RNA samples used in RNA sequencing (Fig. S2).

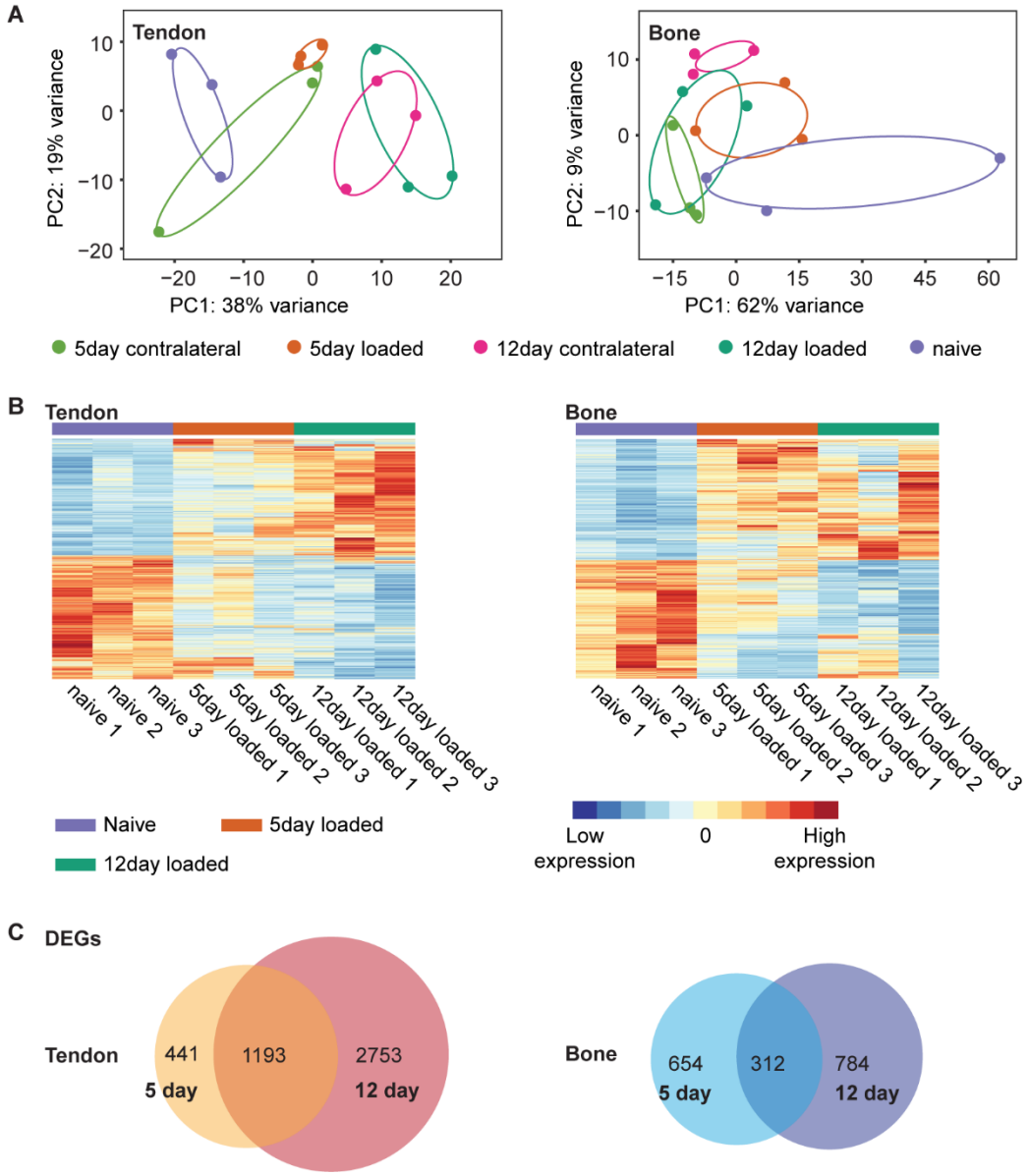

Fig. 4. Optogenetic-induced loading led to transcriptional response in both tendon and bone. (A) Principal component analysis plots of differential gene expression for naïve, contralateral, and loaded tendons and bones after 5day and 12 days of loading. (B) Heatmaps of

all differentially expressed genes for Achilles tendon and calcaneus (bone) in naïve, 5 day loaded, and 12 day loaded mice. (C) In tendon and bone 1,193 and 312 genes, respectively, were differentially expressed after 5 and 12 days of loading. DEGs were identified using Wald test in R/Bioconductor/DESeq2 with Benjamini-Hochberg p-adj < 0.05. N=15 per tissue.

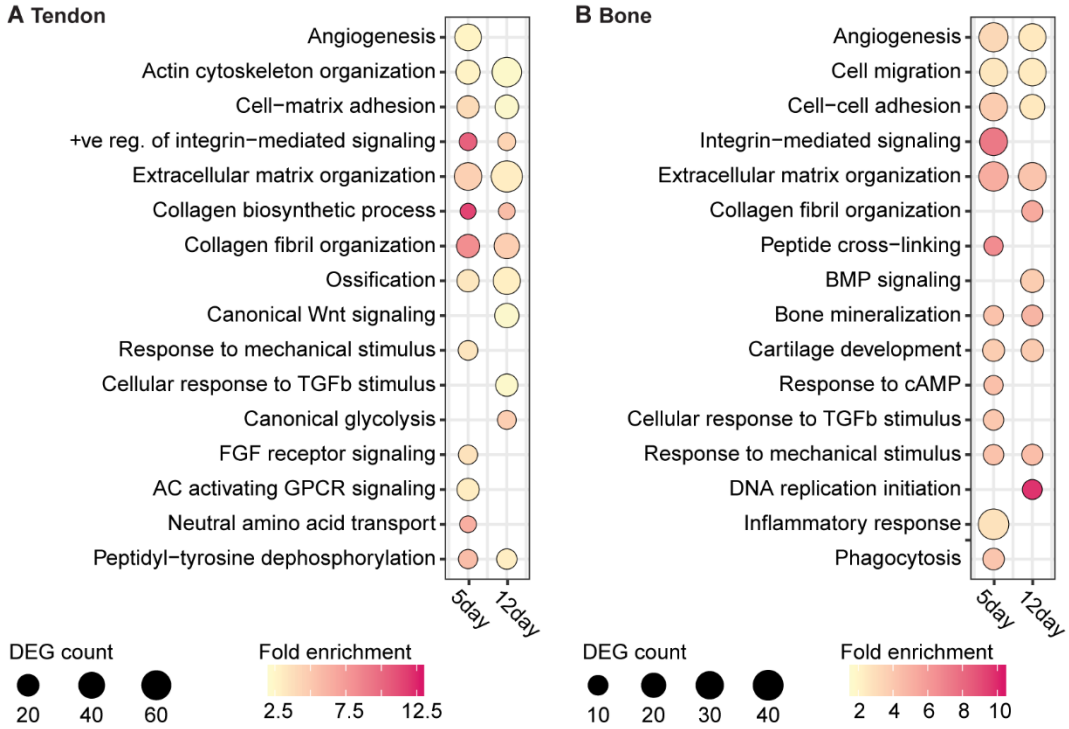

Fig. 5. Relevant biological processes that were differentially regulated by optogenetically-induced loading in Young (A) Achilles tendon and (B) bone (calcaneus). Loading enriched processes related to cell adhesion, cytoskeleton and ECM regulation, mechanotransduction, and ossification in both tissues. Biological processes were identified using DAVID's statistical test of overrepresentation with false discovery rate (FDR) < 0.05 and enrichment > 1.5.

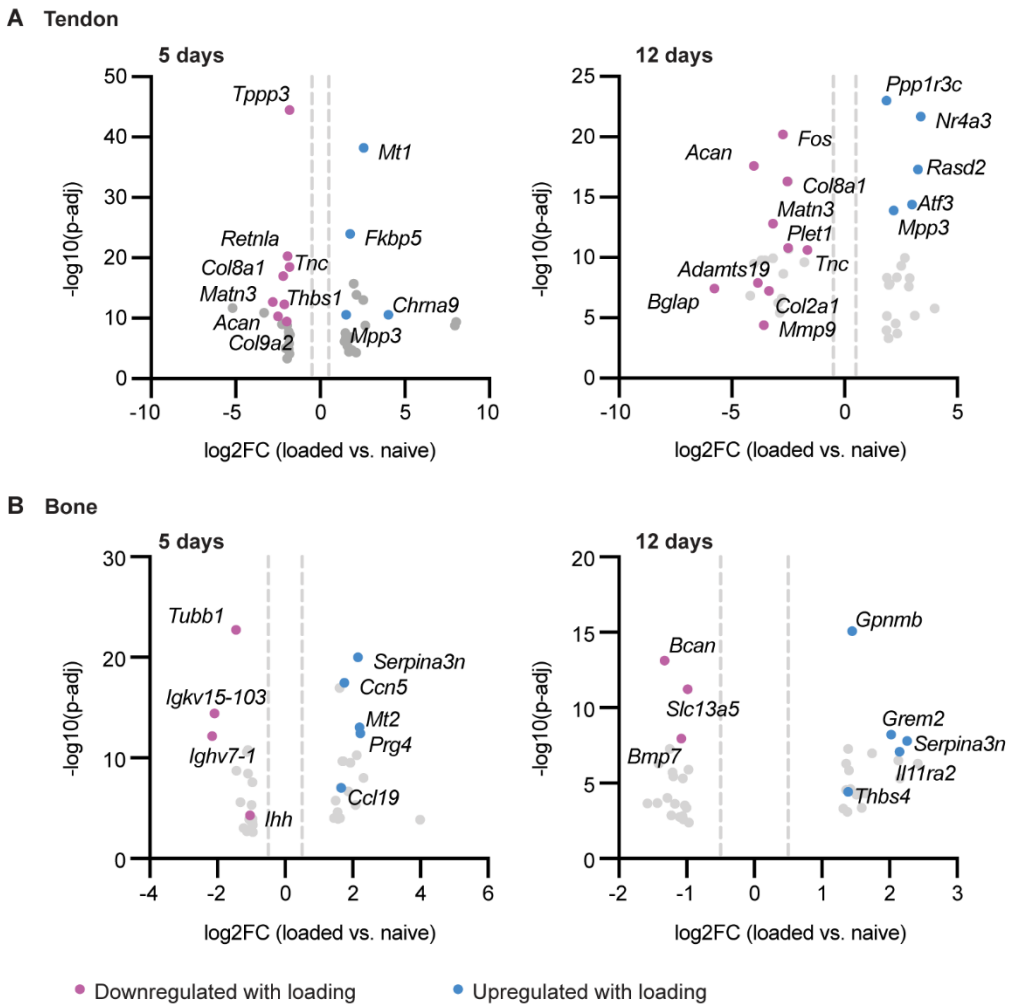

Fig. 6. After 5 days and 12 days of stimulation, daily bouts of optogenetic loading led to significant downregulation of genes associated with tendon stem cell activation and ECM synthesis in tendon and upregulation of proinflammatory markers in bone. Data shown are log2 transformed fold change (log2FC, x-axis) and -log10 transformed p-adj (-log10(p-adj), y-axis). Dashed lines: ±0.5 log2FC.

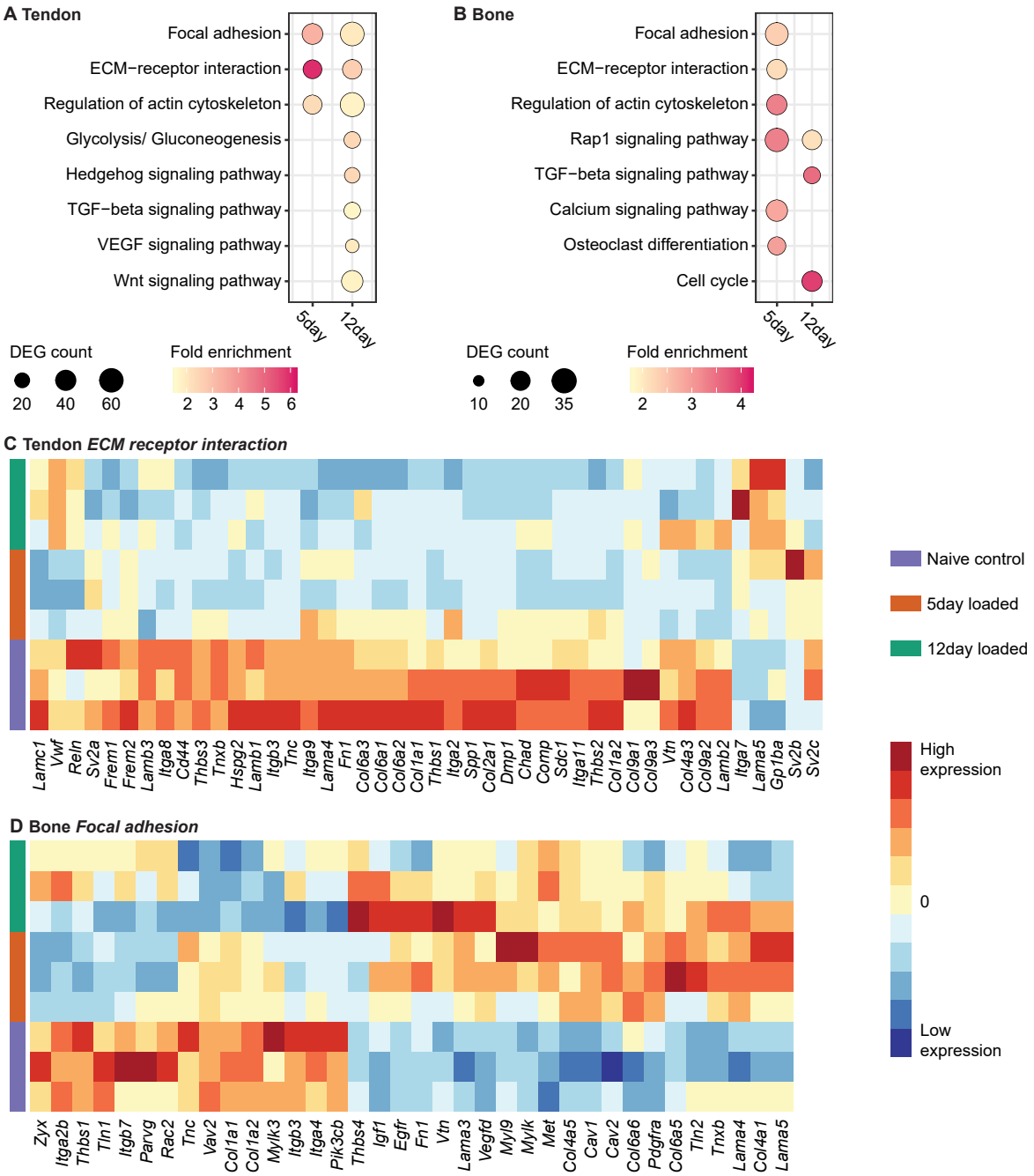

Fig. 7. Relevant KEGG pathways that were differentially regulated by optogenetics-induced loading in Young (A) Achilles tendon and (B) bone (calcaneus). (C) ECM receptor interaction pathway in tendon is driven by 44 genes of which > 90% are downregulated with loading while in (D) calcaneus focal adhesion pathway is driven by 36 genes of which > 50% are upregulated with loading. Pathways were identified using DAVID's statistical test of overrepresentation with FDR < 0.05 and enrichment > 1.5.

Discussion

In this study, we evaluated the mechanically induced adaptation of both the young and adult enthesis to repeated loading using optogenetic stimulation. Previous studies have explored the effects of repeated loading on the structural and functional adaptation of healthy and repaired tendon and enthesis in adult and aging tissues (*29*, *49–52*). Yet, the effect of repeated loading on immature tendon and enthesis was previously unknown. We used optogenetic stimulation of triceps surae muscle to induce ankle joint plantar flexion with comparable generated joint torques to electrically-induced nerve stimulation (*44*). We leveraged pulsatile light-induced activation of ChR2 in skeletal muscle cells for repeated tensile loading of the Achilles tendon and enthesis. Optogenetic activation of skeletal muscle was non-invasive and did not cause weight loss or gross macroscopic damage to the tendon or enthesis after 3 weeks. Repeated loading did result in microscopic changes and disruption of the structure and function of the young, but not the adult enthesis. Repeated loading also led to opening of the growth plate, disruption of the enthesis tidemark, and impaired mechanical properties in Young mice. This may have been caused by disruption of the continuous transition between the mineralized and unmineralized fibrocartilage of the enthesis that contributes to the tissue's mechanical toughness (*53*) and is the primary determinant of enthesis mechanics and stress transfer between tendon and bone (*54*).

In tendons, aging leads to impaired self-renewal potential (*55*), tissue turnover (*56*), increased prevalence of proteoglycans and mineral (*57*), and degenerative structural adaptations (e.g., reduced cellularity, disruption collagen fiber orientation, and fibroblastic changes) (*56*, *57*). In mice, reduced tendon stem cell proliferation has been reported as early as 5 months of age (*55*). In previous studies, degenerative changes of the adult tendon and enthesis in response to increased loading include increased cross-sectional area (*29*), higher cellularity (*49*, *51*), neovascularization (*49*), and reduced fiber organization (*29*, *49*, *51*). Excessive repeated loading can also lead to reduced stiffness and strength (*52*). However, in our study, repeated muscle-induced loading of the adult enthesis did not lead to pathological adaptation. This could be a result of physiological and isometric loading or post-loading compensatory recovery after dosing.

Increased and repeated loading leads to dose-dependent degeneration by the accumulation of sub-failure damage. Collagen is the primary stabilizing constituent of the tendon, bone, and

enthesis ECM and the key contributing factor to the elastic behavior of tendon (*58*) and toughness of the bone (*59*). In the tendon, structural reorganization of collagen fibers can be exacerbated into non-reversible molecular level denaturation of the collagen fiber collagen, ultimately leading to inferior mechanical properties (*46*). Collagen hybridizing peptides (CHPs) are synthetic single strand peptides that have recently been developed to hybridize with denatured collagen triple helix. In tendon, CHPs can specifically bind to non-recoverable (post-yield) sites of collagen fibril unfolding (*27*, *46*). Enzymatic and mechanical factors drive tendon ECM degradation and remodeling processes (*60*). In the present study, we found that repeated loading did not result in upregulation of genes associated with matrix metalloproteinases; rather, loading downregulated *Mmp9* as well as several other genes associated with ECM remodeling. These findings suggest that the increased *in vivo* labeling of the Achilles tendon with CHPs may be caused by increased collagen denaturation, rather than enzymatic degradation. Similar to findings from repeatedly loaded tendon *ex vivo* (*61*), our results show that loading-induced collagen denaturation does not coincide with altered tissue stiffness. These findings suggest a compensatory mechanism (e.g., collagen fiber sliding) rather than a fiber-dominant pre-yield mechanism of load transfer in the tendon and enthesis. Alternatively, repeated loading in growing enthesis leads to reduced mineral deposition at subchondral and apophyseal bone and disruption of ECM composition in young enthesis that functionally translate to significant decrease of enthesis toughness and tensile strength. These results are in agreement with the role of mineral as the primary toughening constituent of the enthesis (*4*).

The ECM disruption and altered calcaneal shape in the Young loaded calcaneus suggests an unexplored role of mechanical loading in enthesis and apophysis adaptation during growth. The role of increased loading on the formation and maturation of the mineralizing growth plate during postnatal maturation was elucidated in our bulk RNAseq studies, and we identified key pathways that are transcriptionally activated in the growing calcaneus as well as tendon. We observed downregulation of genes associated with mechanosensitive pathways and processes, such as ECM receptor interaction, focal adhesion etc. Overuse of tendon can disrupt

mechanotransduction by altering cell signaling structures and surrounding matrix environment (*62*). Type VI collagen and type II fibrillin, two major constituents of tenocyte pericellular matrix (*63*) were consistently downregulated with loading, indicating that tendon overloading, and associated ECM disruption may have compromised the interaction between the cell and ECM (*62*, *64*). Sun et al showed that expression of integrins in tendon did not correlate with the increase of loading dose, suggesting an overuse-induced ECM damage that regulates mechanosensitivity (*65*). Our findings model the structural and mechanical changes similar to those occurring in pediatric apophyseal pathologies and in the young athletes (*66*, *67*). This study provides the first small animal model of pediatric apophyseal pathologies that can be leveraged for future systematic examination of mechanisms of injury and repair in growing skeleton. Establishing the time course of gene expression of mechanosensitive pathways following loading and during key periods of remodeling will be important next steps for future studies.

Although muscle contraction was confirmed throughout the experimental loading duration, the translated loads from muscle to tendon, enthesis, and bone during loading are unknown. Berman et al. showed that comparable ankle torques to what we measured can induce osteogenic strains in the tibial mid-diaphysis in adult mice (*68*). Additionally, step cycle and triceps surae activation durations were previously reported as approximately 300-400ms in adult C57BL6J mice (*69*, *70*). In this study, we have used optical stimulation at supraphysiological duration of 1000ms and 10Hz optical cell activation frequency, which is within and in the lower range of motor unit frequencies in the triceps surae muscle in adult mice (*71*). Future studies should investigate ways to improve transgenic strains for sustained contractile fusion using optogenetic stimulation. Finally, there may be unknown physiological changes that directly or indirectly affect the mechanoadaptation of the tendon and enthesis.

In summary, this work provides a new understanding of enthesis and calcaneal bone adaptation to mechanical loading, induced by optogenetic control of skeletal muscle contraction. This useful tool to control tendon, enthesis, and bone loading is advantageous for understanding

mechanobiology of the immature musculoskeleton that provides an easily translatable approach to other anatomical sites.

Materials and Methods

All procedures were approved by the Institutional Animal Care and Use Committees at the University of Delaware (AUP 1296) and the University of Michigan (PRO00009507). Doxycycline-inducible ACTA1-rtTA;tetO-cre mice (Acta1-Cre; C57BL6J background; Jax ID: 012433) and Ai32 reporter mice (Jax ID: 024109, C57BL6J background) were obtained from Jackson Laboratory (Bar Harbor, ME, USA). Acta1-Cre and Ai32 reporter mice were bred to generate F2 (Ai32 homozygous) lines that expressed a YFP-fused ChR2 light-sensitive opsin (455nm sensitivity) in skeletal muscle when treated with tetracycline. Dams were treated with doxycycline chow at the time of mating and maintained on chow until offspring were weaned. Previously, we have shown that the muscle-specific and nerve-independent expression of ChR2-EYFP is maintained in adult mice (up to 6-months-old offspring) when treated with doxycycline during gestation and prior to weaning only (*44*). Offspring were genotyped using PCR (Transnetyx, Cordova, TN, USA). A total of 57 mice were used in this study. Mice were randomized across various experiments. ActaCre;Ai32 homozygous mice (n=38 total) were used for unilateral light-induced stimulation of muscle in Young (3-4 weeks old, n = 30; 12 females and 18 males) or Adult (6-8 months old, n = 8; 2 females and 6 males) mice. Contralateral (within-animal) limbs were used as paired controls. Additionally, a second group of ActaCre; Ai32 mice was used to compare age-matched littermates as naïve controls for both Young (n = 11; 5 females and 6 males) and Adult (n = 4; 2 females and 2 males) groups (Fig. 6). An additional 3-month-old ActaCre;Ai32 mouse was used to test muscle contractility response to blue light *in vitro*. Unless otherwise stated, all animals were included for respective analyses described below.

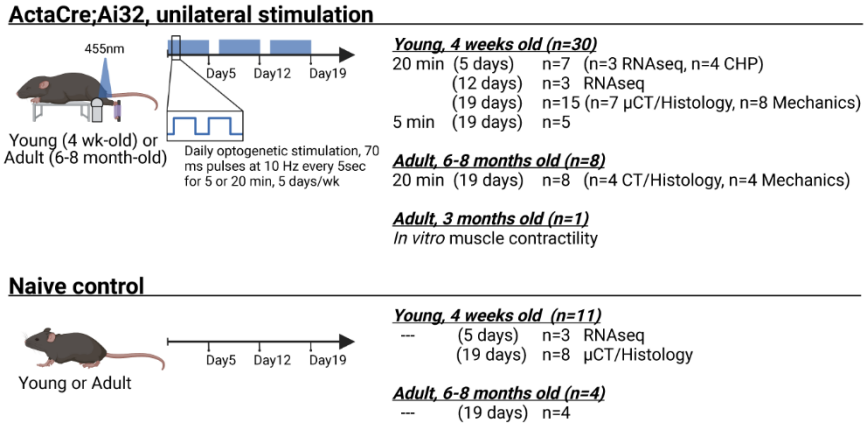

Fig. 8. Study design. Schematic of experimental setup for optogenetic muscle loading (shown here for young mice). Right hindlimbs of Young and Adult ActaCre;Ai32 mice were exposed to daily bouts of either 5- or 20-minute optogenetic-induced muscle contractions of the triceps surae. Mice were used experimentally after various loading bouts, including for RNA sequencing (Young mice only; after 5 or 12 days of 20min loading); for collagen damage assays (CHP; Young mice only, after 5 days of 20min loading); for microcomputed tomography (Young and Adult mice; 19 days of 20min loading); and for mechanical testing (Young and Adult mice; 19 days of 20min loading). At each designated endpoint (i.e., experimental days 5, 12, or 19), experimental and naïve age-matched controls were euthanized to collect Achilles tendon and enthesis for histology, µCT, and mechanics and Achilles tendon and calcaneus for RNA isolation (RNAseq).

Optogenetics stimulation for daily tendon enthesis loading

Mice were anesthetized with isoflurane, and hair was removed using chemical hair remover from their right triceps surae muscles (Nair, Church & Dwight, Ewing, NJ, USA). Animals were placed on a heating pad in prone position and body temperature was maintained at 37°C (Stoeling, Wooddale, Il, USA). The right limb was stabilized at the knee joint with a clamp, and the right foot was placed on a foot pedal for isometric muscle stimulation. Animals were weighed daily before stimulations. For light stimulation, a collimated LED light (455 nm, 900 mW, M455L3, Thorlabs) and a high-power LED driver (DC2200, Thorlabs, Newton, NJ) were used for pulse modulation (*44*). Driver code was adjusted in LabView (National Instruments, Austin, TX, USA) to add pulsatile light activation and deactivation controls (bouts of stimulation and rest) for the period of experiment. Light source was placed above the triceps surae muscles at a distance to induce ~0.3 mW/mm^2 light intensity. Triceps surae muscles were stimulated using an approximated 10Hz pulsed light (70ms on, 30ms off; 10 cycles) followed by 4 seconds of rest for 20 minutes (240 consecutive loading cycles) in Young (n = 27, 12 females and 15 males) and Adult (n = 8, 2 females and 6 males) groups. Daily bouts of loading were repeated

weekly with five days of stimulation and two days of rest for up to 3 weeks (19 days). A subset of these mice in the Young group (n=7) were also used to measure ankle torque throughout the stimulation using servomotor shaft (Aurora 3-in-1 system, Aurora Scientific, Ontario, Canada) that was connected to the foot pedal. All other mice were loaded in a 3D printed mimic of the platform. Knee and ankle placements were replicated for the Young Control group for 20 minutes daily under anesthesia. After recovery from anesthesia, mice were returned to their cages for unrestricted cage activity. An additional cohort of Young mice were added to compare the effects of bout duration (5 minutes "short" loading; 60 consecutive cycles; n = 5, 2 females and 3 males) loading duration on weight gain over the three week duration of the experiment.

In vitro contractility with optogenetic stimulation

Right EDL muscles were dissected from 3-month-old ActaCre;Ai32 mice (doxycycline removed at 3wks of age) and were and placed in buffered Ringer's solution bath. Distal and proximal tendons of EDL were tied with sutures to a fixed post and force transducer (BG-50, Kulite Semiconductor), respectively (*72*). Blue light (455 nm LED; ~140mW/cm2; Thorlabs) was shone on the muscle to evoke optogenetic twitches. Forces were recorded with incremental light pulse duration ranging from 5 to 70 ms.

Micro-computed tomography

Mice were euthanized using carbon dioxide asphyxiation 48 hr after the final bout of loading. The skin was carefully dissected, and distal hindlimbs (knee, ankle, and foot) were fixed for 24 hr in 4% paraformaldehyde. Calcaneus-tibial complexes were scanned using micro-computed tomography (microCT) at the University of Delaware (microCT, Bruker SkyScan 1276; 59kV, 175µA, 10.58µm voxel size, 930ms exposure, 0.5mm aluminum filter).

Bone morphometry and statistical shape modeling

Aligned image stacks were reconstructed at the University of Michigan for qualitative and quantitative assessment of calcaneal bone shape using Dragonfly software (v2022.2, Object Research Systems, Montreal, Quebec). After reconstruction, the calcaneus was aligned vertically along its long axis and transversely cropped to include the peroneal tubercle. Bone morphometry was assessed within this volume after applying a median filter in 3D (square median kernel size =3) and "split at Otsu" to identify bone and non-bone regions. We then calculated tissue volume (TV), bone volume (BV), and bone volume percentage (BV/TV) for bone morphometry. To generate solid objects for use in statistical shape modeling, we digitally cleaned the regions of

interests (ROIs) to remove other bones and filled the growth plate and trabecular/marrow cavities (complete fill) in Dragonfly. ROIs from left (control) image datasets were mirrored to anatomically mimic right (loaded) image datasets for shape modeling. We then created a mesh and imported STL files into ShapeWorks Studio (6.3.2, http://shapeworks.sci.utah.edu). Shapes were groomed to fill holes, smooth (Laplacian, 10 iterations, relaxation = 1), remeshed (75% number of vertices and 1.00 adaptivity) and aligned (based on three anatomical landmarks at processes of the calcaneal tuberosity). Optimization was performed using the following settings: number of particles = 512; initial relative weighting = 1; relative weighting = 200; starting/ending regularization = 1000; iterations per split = 1000; optimization iterations = 1000; Procrustes rotation/translation = yes; Procrustes interval = 10; narrow band = 4. Quality was assessed via metrics (compactness, specificity, and generalization) for shape modes and principal component analyses were evaluated for Young shapes only (control vs. loaded) because of limited sample size in the Adult group. Deformation maps were generated to visualize shape changes from the mean shape of the control group to mean shape of the loaded group, with growth or loss in response to loading shown in red or blue, respectively. Comparisons were made between Young (loading started at 4wk of age; control and loaded) samples from 20min bouts (3wk duration; n=7 control and n=7 loaded) and between Adult (control and loaded) samples from 20min bouts (3wk duration; n=4 control and n=4 loaded). Due to low sample size (n=4), statistical shape analyses were not performed on adult mice.

Histology

Distal hindlimbs from mice treated with 20-minute of loading for 3 weeks (19 days) as well as from naïve controls were decalcified in 14% ethylenediaminetetraacetic acid and processed for paraffin embedding. Tissues were sectioned at 6μm in the sagittal plane and stained with Hematoxylin and Eosin (H&E) or Toluidine Blue and cover-slipped with an acrylic mounting media (Acrymount, Statlab, McKinnery, TX, USA) or used for immunohistochemistry. For immunohistochemistry, paraffin sections were deparaffinized and quenched in 0.3% hydrogen peroxide (Santa Cruz, Dallas, TX), followed by heat-mediated antigen retrieval, and blocking (5% goat serum in phosphate buffer saline). Slides were then incubated in primary antibodies (listed in Table 1) overnight at 4°C, followed by washing and incubation with appropriate secondary antibodies. Horseradish peroxidase 3,3'-Diaminobenzidine system (Millipore Sigma, Billerica, MA, USA) was used for detection, slides were counterstained with Hematoxylin, and

coverslipped with Acrymount (Acrymount, Statlab, McKinney, TX, USA). All slides were imaged on a brightfield microscope (Eclipse Ni-U, Nikon).

Biomechanical testing of the Achilles enthesis

After 3 weeks of daily (20min; 5 consecutive days per week) loading, Young and Adult mice were euthanized, and carcasses were stored intact at -20°C until testing. Carcasses were thawed at 4°C for no more than 24 hr and Achilles tendon-calcaneus complex was carefully dissected and stored in PBS for no more than 2 hr at room temperature. Before mechanical testing, the muscle was carefully dissected from the Achilles tendon, the plantaris tendon was detached, and the calcaneus was disarticulated from the foot. Cross-sectional area (CSA) measurements were made using photogrammetry with a custom 3D-printed fixture attached to a motor controller (Arduino, Ivrea, Italy). Forty consecutive images of the tendon-bone complex were acquired at 9-degree rotation steps using a macro lens (Basler Fujinon Lens, Ahrensburg, Germany). Images were converted from sparse to dense point clouds, and an STL surface mesh of the tendon was generated using Metashape software (Agisoft, St. Petersburg, Russia). CSA was measured using Dragonfly software at the Achilles tendon near the enthesis. The calcaneus was then placed in a custom 3D printed fixture to secure the bone (FormLabs 3B, Somerville, MA, USA), and the proximal Achilles tendon was clamped in a thin film grip (Imada, Northbrook, IL, USA) (*73*). The assembled tendon-grip unit was placed in a custom PBS bath maintained at 37ºC via a temperature controller (MA160, Biomomentum Inc, Laval, Quebec, Canada) and secured with a pin to a tensile testing frame with multi-axis load cells (Mach-1 VS500CST, ±70N, Biomomentum, Laval, Quebec, Canada). Samples were preloaded to 0.01N, and gauge length (L_0) was measured (4.01 ± 0.17 mm) as the distance between the calcaneal fixture and the thin film grip. Tendons were preconditioned for 10 cycles (±0.05N at 0.03 Hz) followed by load to failure at 0.05mm/sec. Load and torque data (6 degrees of freedom) were collected to assess off-axis loading for the duration of the experiment. Using Mach-1 Analysis and custom Matlab script (R2017 or later, Mathworks, Natick, USA), mechanical properties of the entheses were calculated from force-displacement data. Engineering stress was calculated as the instantaneous force divided by the original CSA (calculated from photogrammetry). Instantaneous grip-to-grip strain was calculated as the displacement divided by original gauge length, L_0. Stiffness and elastic modulus were calculated from the linear portion of the load-displacement and stress-strain curves, respectively. Maximum load, maximum stress, and maximum strain were calculated, as

well as work to maximum force (area under the curve, AUC) and toughness from the area under the force-displacement and stress-strain curves. Maximum strain was calculated as the strain at maximum force.

Collagen hybridization and damage visualization

Young mice were loaded for 20 minutes daily for 5 days (n=4). Immediately following the last bout of loading, 20µl sulfo-Cy7.5 collagen hybridizing peptide (sCy7.5-CHP) (3Helix, Salt Lake City, UT, USA) was injected subcutaneously adjacent to the Achilles tendon mid-substance using an insulin syringe (Exel International, CA, USA). Mice were imaged under anesthesia (Li-Cor Pearl imager; 85 µm pixel resolution; 700 and 800 nm wavelength) 24 hours after the injection. Intensity measurements were taken in a user-defined ROI at the Achilles tendon and enthesis, using Li-Cor image acquisition software for both 700 and 800 nm wavelengths.

RNA-sequencing of tendon and bone

Young mice were euthanized 4 hr after the 5th or 12th consecutive day of loading and tendon and calcaneal bone from loaded and contralateral (not loaded) limb were immediately dissected under RNase-free conditions and snap froze (n=3 male mice per time point). Age-matched Achilles tendons and calcaneal bones were also collected as a naïve control group (n=3 male mice; age matched to the 5th consecutive day time point). Tissues were mechanically pulverized in Trizol and total RNA was isolated using spin-columns (PureLink RNA mini kit, Thermo Fisher Scientific) with on column genomic DNA digestion (RNase free DNase, Qiagen). RIN was measured using Bioanalyzer (Agilent). Poly-A mRNA libraries were prepared and next-generation sequencing was performed using Illumina NovaSeq Shared platform. Reads were mapped to the genome reference consortium mouse build 38 (GRCm38). Differential gene expression was determined from count matrices with either paired design (loaded vs. contralateral) or unpaired design (loaded ~~or contralateral~~ vs. naïve control) in DESeq2 in R/Bioconductor (*74*).

Gene expression verification with qRTPCR

We verified gene expression of 4 genes that were differentially expressed in tendon with loading: *Tnc*, *Col1a1*, *Col1a2*, and *Col2a1* (Integrated DNA Technologies) with qRTPCR. Redundant RNA following sequencing from naïve, 5day loaded, and 12day loaded samples (n=3 per group) was reverse transcribed to cDNA (SuperScript IV VILO Master Mix, Thermo Fisher Scientific). Quality and quantity of RNA were checked with NanoDrop spectrophotometer

(Thermo Fisher Scientific) prior to conversion. qRTPCR was performed in CFX96 Real-Time PCR Detection System (Bio-Rad) with Power SYBR Green PCR Master Mix (Thermo Fisher Scientific). *B2m* was used as the reference gene. Primer information are provided in Table 1.

Statistical analysis

Statistical comparisons were performed using Prism (8.3 or higher, GraphPad Software, La Jolla, USA) or in R (version 4.1.0). Gaussian distribution of the data was evaluated using Shapiro-Walik and D'Agostino-Pearson normality tests. Results from micro-CT analyses were tested for normality and compared between the loaded and control samples using an unpaired t-tests. For statistical comparison of the CSA measurements and mechanical testing results, parametric data were tested using paired two-tailed t-test, and Wilcoxon rank test was used for non-parametric results. To identify DEGs, we used Wald test of significance and corrected p-values for multiple testing using the Benjamini and Hochberg method (p-adj < 0.05). Log2FCs were shrunk to account for high dispersion and low counts (*75*). Median ratio algorithm of DESeq2 was used to normalize counts for sequencing depth and gene length (*76*). For functional annotation, list of DEGs with $|\log2FC| \geq 0.32$ were input separately for each time point and tissue into DAVID (*77*, *78*) with *Mus musculus* background. Gene ontology biological processes and KEGG pathways were obtained with FDR < 0.05 and fold enrichment ≥ 1.5. For power analysis, the effect size was calculated from the descriptive statistics of each group, and the effect size was calculated as the ratio of mean and standard deviation (SD) of difference. Power for each variable was calculated using total sample size (N=16), significance (α=0.05), and the calculated effect size for a t-test with match mean values. For power < 0.8, a priori power analysis was performed to calculate the required sample size to achieve 0.8 power. For most outcomes, statistical significance was considered as p = or < 0.05. Mean ± SD are reported. All images were de-identified and analyzed by at least one blinded reviewer, and results were aggregated by one of the lead authors (SNL, EG, or MLK) for sorting.

Table 1. Antigen retrieval and antibody information for immunohistochemistry experiments.

Antibody	Source and Catalog #	Dilution	Buffer; Antigen Retrieval
Anti-Collagen III (rabbit polyclonal)	Abcam, ab7778	1:100	Tris EDTA, pH 9.0; 65°C, 2hr
Anti-Aggrecan (rabbit polyclonal)	Abcam, ab216965	1:100	0.1% tryps in; 37°C, 30 min
Biotinylated goat anti-mouse IgG	Millipore-Sigma, 20777	1:1000	Room temperature, 10 minutes
Biotinylated goat anti-rabbit IgG	Millipore-Sigma, 20715	1:1000	Room temperature, 10 minutes

Primer	Version	Company	Assay ID
Tnc	PrimeTime® qPCR Primers	IDT	Mm.PT.58.8090418
Col1a1	PrimeTime® qPCR Primers	IDT	Mm.PT.58.7562513
Col1a2	PrimeTime® qPCR Primers	IDT	Mm.PT.58.5206680
Col2a1	PrimeTime® qPCR Primers	IDT	Mm.PT.58.10123677
B2m	PrimeTime® qPCR Primers	IDT	Mm.PT.39a.22214835

References

1. L. Rossetti, L. A. Kuntz, E. Kunold, J. Schock, K. W. Müller, H. Grabmayr, J. Stolberg-Stolberg, F. Pfeiffer, S. A. Sieber, R. Burgkart, A. R. Bausch, The microstructure and micromechanics of the tendon–bone insertion. *Nature Materials*. **16**, 664–670 (2017).
2. M. Benjamin, D. McGonagle, "The Enthesis Organ Concept and Its Relevance to the Spondyloarthropathies" in *Molecular Mechanisms of Spondyloarthropathies*, C. López-Larrea, R. Díaz-Peña, Eds. (Springer, New York, NY, 2009; https://doi.org/10.1007/978-1-4419-0298-6_4), *Advances in Experimental Medicine and Biology*, pp. 57–70.
3. S. Thomopoulos, J. P. Marquez, B. Weinberger, V. Birman, G. M. Genin, Collagen fiber orientation at the tendon to bone insertion and its influence on stress concentrations. *Journal of Biomechanics*. **39**, 1842–1851 (2006).
4. M. Golman, A. C. Abraham, I. Kurtaliaj, B. P. Marshall, Y. J. Hu, A. G. Schwartz, X. E. Guo, V. Birman, P. J. Thurner, G. M. Genin, S. Thomopoulos, Toughening mechanisms for the attachment of architectured materials: The mechanics of the tendon enthesis. *Science Advances*. **7**, eabi5584 (2021).
5. G. M. Genin, S. Thomopoulos, Unification through disarray. *Nature Materials*. **16**, 607–608 (2017).
6. J. M. Weatherall, K. Mroczek, N. Tejwani, Acute achilles tendon ruptures. *Orthopedics*. **33**, 758–764 (2010).
7. J. A. Ogden, T. M. Ganey, J. D. Hill, J. I. Jaakkola, Sever's injury: a stress fracture of the immature calcaneal metaphysis. *Journal of Pediatric Orthopedics*. **24**, 488–492 (2004).
8. M. M. Duong, A. D. Nicholson, S. Q. Li, A. Gilmore, D. R. Cooperman, R. W. Liu, Relationship Between Sever Disease and Skeletal Maturity. *Journal of Pediatric Orthopaedics*. **40**, 93–96 (2020).
9. M. Benjamin, H. Toumi, J. R. Ralphs, G. Bydder, T. M. Best, S. Milz, Where tendons and ligaments meet bone: attachment sites ('entheses') in relation to exercise and/or mechanical load. *Journal of Anatomy*. **208**, 471–490 (2006).
10. N. Maffulli, J. Wong, L. C. Almekinders, Types and epidemiology of tendinopathy. *Clinics in Sports Medicine*. **22**, 675–692 (2003).
11. C. E. Shopfner, C. G. Coin, Effect of Weight-Bearing on the Appearance and Development of the Secondary Calcaneal Epiphysis. *Radiology*. **86**, 201–206 (1966).

12. M. Kvist, Achilles tendon injuries in athletes. *Annales Chirurgiae Et Gynaecologiae*. **80**, 188–201 (1991).

13. J. I. Wiegerinck, R. Zwiers, I. N. Sierevelt, H. C. P. M. van Weert, C. N. van Dijk, P. A. A. Struijs, Treatment of Calcaneal Apophysitis: Wait and See Versus Orthotic Device Versus Physical Therapy: A Pragmatic Therapeutic Randomized Clinical Trial. *Journal of Pediatric Orthopedics*. **36**, 152–157 (2016).

14. A. Schwartz, J. Lipner, J. Pasteris, G. Genin, S. Thomopoulos, Muscle loading is necessary for the formation of a functional tendon enthesis. *Bone*. **55**, 44–51 (2013).

15. M. L. Killian, S. Thomopoulos, Scleraxis is required for the development of a functional tendon enthesis. *The FASEB Journal*. **30**, 301–311 (2016).

16. M. L. Killian, Growth and mechanobiology of the tendon-bone enthesis. *Seminars in Cell & Developmental Biology*. **123**, 64–73 (2022).

17. E. Blitz, S. Viukov, A. Sharir, Y. Shwartz, J. L. Galloway, B. A. Pryce, R. L. Johnson, C. J. Tabin, R. Schweitzer, E. Zelzer, Bone Ridge Patterning during Musculoskeletal Assembly Is Mediated through SCX Regulation of Bmp4 at the Tendon-Skeleton Junction. *Developmental Cell*. **17**, 861–873 (2009).

18. H. M. Shaw, M. Benjamin, Structure-function relationships of entheses in relation to mechanical load and exercise: Tendon and ligament entheses. *Scandinavian Journal of Medicine & Science in Sports*. **17**, 303–315 (2007).

19. J. Kahn, Y. Shwartz, E. Blitz, S. Krief, A. Sharir, Dario. A. Breitel, R. Rattenbach, F. Relaix, P. Maire, R. B. Rountree, D. M. Kingsley, E. Zelzer, Muscle Contraction Is Necessary to Maintain Joint Progenitor Cell Fate. *Developmental Cell*. **16**, 734–743 (2009).

20. I. Rot-Nikcevic, T. Reddy, K. J. Downing, A. C. Belliveau, B. Hallgrímsson, B. K. Hall, B. Kablar, Myf5 −/− :MyoD −/− amyogenic fetuses reveal the importance of early contraction and static loading by striated muscle in mouse skeletogenesis. *Development Genes and Evolution*. **216**, 1–9 (2006).

21. S. Achar, J. Yamanaka, Apophysitis and Osteochondrosis: Common Causes of Pain in Growing Bones. *American Family Physician*. **99**, 610–618 (2019).

22. M. E. Lynch, R. P. Main, Q. Xu, D. J. Walsh, M. B. Schaffler, T. M. Wright, M. C. H. van der Meulen, Cancellous bone adaptation to tibial compression is not sex dependent in growing mice. *Journal of Applied Physiology*. **109**, 685–691 (2010).

23. R. L. De Souza, M. Matsuura, F. Eckstein, S. C. F. Rawlinson, L. E. Lanyon, A. A. Pitsillides, Non-invasive axial loading of mouse tibiae increases cortical bone formation and modifies trabecular organization: A new model to study cortical and cancellous compartments in a single loaded element. *Bone*. **37**, 810–818 (2005).

24. T. K. Patel, M. D. Brodt, M. J. Silva, Experimental and finite element analysis of strains induced by axial tibial compression in young-adult and old female C57Bl/6 mice. *Journal of Biomechanics*. **47**, 451–457 (2014).

25. S. P. Kotha, Y.-F. Hsieh, R. M. Strigel, R. Müller, M. J. Silva, Experimental and finite element analysis of the rat ulnar loading model—correlations between strain and bone formation following fatigue loading. *Journal of Biomechanics*. **37**, 541–548 (2004).

26. A. G. Robling, F. M. Hinant, D. B. Burr, C. H. Turner, Improved Bone Structure and Strength After Long-Term Mechanical Loading Is Greatest if Loading Is Separated Into Short Bouts. *Journal of Bone and Mineral Research*. **17**, 1545–1554 (2002).

27. D. T. Fung, V. M. Wang, N. Andarawis-Puri, J. Basta-Pljakic, Y. Li, D. M. Laudier, H. B. Sun, K. J. Jepsen, M. B. Schaffler, E. L. Flatow, Early response to tendon fatigue damage accumulation in a novel in vivo model. *Journal of Biomechanics*. **43**, 274–279 (2010).

28. J. B. Sereysky, N. Andarawis-Puri, K. J. Jepsen, E. L. Flatow, Structural and mechanical effects of in vivo fatigue damage induction on murine tendon. *J. Orthop. Res.* **30**, 965–972 (2012).

29. L. J. Soslowsky, S. Thomopoulos, S. Tun, C. L. Flanagan, C. C. Keefer, J. Mastaw, J. E. Carpenter, Neer Award 1999: Overuse activity injures the supraspinatus tendon in an animal model: A histologic and biomechanical study. *Journal of Shoulder and Elbow Surgery*. **9**, 79–84 (2000).

30. A. C. Abraham, S. A. Shah, M. Golman, L. Song, X. Li, I. Kurtaliaj, M. Akbar, N. L. Millar, Y. Abu-Amer, L. M. Galatz, S. Thomopoulos, Targeting the NF-κB signaling pathway in chronic tendon disease. *Science Translational Medicine*. **11** (2019), doi:10.1126/scitranslmed.aav4319.

31. B. P. Thampatty, J. H.-C. Wang, Mechanobiology of young and aging tendons: In vivo studies with treadmill running. *Journal of Orthopaedic Research: Official Publication of the Orthopaedic Research Society*. **36**, 557–565 (2018).

32. A. C. Abraham, F. Fang, M. Golman, P. Oikonomou, S. Thomopoulos, The role of loading in murine models of rotator cuff disease. *Journal of Orthopaedic Research*. **40**, 977–986 (2022).
33. Y. J. Kim, H. J. Kim, W. J. Lee, J. K. Seong, A comparison of the metabolic effects of treadmill and wheel running exercise in mouse model. *Laboratory Animal Research*. **36**, 3 (2020).
34. I. Lerman, B. C. Harrison, K. Freeman, T. E. Hewett, D. L. Allen, J. Robbins, L. A. Leinwand, Genetic variability in forced and voluntary endurance exercise performance in seven inbred mouse strains. *Journal of Applied Physiology*. **92**, 2245–2255 (2002).
35. M. Svensson, P. Rosvall, A. Boza-Serrano, E. Andersson, J. Lexell, T. Deierborg, Forced treadmill exercise can induce stress and increase neuronal damage in a mouse model of global cerebral ischemia. *Neurobiology of Stress*. **5**, 8–18 (2016).
36. L. G. Koch, O. J. Kemi, N. Qi, S. X. Leng, P. Bijma, L. J. Gilligan, J. E. Wilkinson, H. Wisløff, M. A. Høydal, N. Rolim, P. M. Abadir, E. M. van Grevenhof, G. L. Smith, C. F. Burant, Ø. Ellingsen, S. L. Britton, U. Wisløff, Intrinsic Aerobic Capacity Sets a Divide for Aging and Longevity. *Circulation Research*. **109**, 1162–1172 (2011).
37. S. N. Rezvani, A. E. C. Nichols, R. W. Grange, L. A. Dahlgren, P. G. Brolinson, V. M. Wang, A novel murine muscle loading model to investigate Achilles musculotendinous adaptation. *Journal of Applied Physiology*. **130**, 1043–1051 (2021).
38. L. H. Nakama, K. B. King, S. Abrahamsson, D. M. Rempel, Evidence of tendon microtears due to cyclical loading in an in vivo tendinopathy model. *Journal of Orthopaedic Research*. **23**, 1199–1205 (2005).
39. E. S. Boyden, A history of optogenetics: The development of tools for controlling brain circuits with light. *F1000 Biology Reports*. **3** (2011), doi:10.3410/B3-11.
40. G. Nagel, T. Szellas, W. Huhn, S. Kateriya, N. Adeishvili, P. Berthold, D. Ollig, P. Hegemann, E. Bamberg, Channelrhodopsin-2, a directly light-gated cation-selective membrane channel. *Proceedings of the National Academy of Sciences*. **100**, 13940–13945 (2003).
41. K. Deisseroth, Optogenetics. *Nature Methods*. **8**, 26–29 (2011).
42. E. S. Boyden, F. Zhang, E. Bamberg, G. Nagel, K. Deisseroth, Millisecond-timescale, genetically targeted optical control of neural activity. *Nat Neurosci*. **8**, 1263–1268 (2005).

43. P. Magown, B. Shettar, Y. Zhang, V. F. Rafuse, Direct optical activation of skeletal muscle fibres efficiently controls muscle contraction and attenuates denervation atrophy. *Nat Commun*. **6**, 8506 (2015).
44. E. Ganji, C. S. Chan, C. W. Ward, M. L. Killian, Optogenetic activation of muscle contraction in vivo. *Connect Tissue Res*. **62**, 15–23 (2021).
45. T. Bruegmann, T. van Bremen, C. C. Vogt, T. Send, B. K. Fleischmann, P. Sasse, Optogenetic control of contractile function in skeletal muscle. *Nature Communications*. **6**, 7153 (2015).
46. J. L. Zitnay, Y. Li, Z. Qin, B. H. San, B. Depalle, S. P. Reese, M. J. Buehler, S. M. Yu, J. A. Weiss, Molecular level detection and localization of mechanical damage in collagen enabled by collagen hybridizing peptides. *Nature Communications*. **8**, 14913 (2017).
47. Y. Li, C. A. Foss, D. D. Summerfield, J. J. Doyle, C. M. Torok, H. C. Dietz, M. G. Pomper, S. M. Yu, Targeting collagen strands by photo-triggered triple-helix hybridization. *Proceedings of the National Academy of Sciences of the United States of America*. **109**, 14767–14772 (2012).
48. L. L. Bennink, Y. Li, B. Kim, I. J. Shin, B. H. San, M. Zangari, D. Yoon, S. M. Yu, Visualizing collagen proteolysis by peptide hybridization: From 3D cell culture to in vivo imaging. *Biomaterials*. **183**, 67–76 (2018).
49. X. Lin, M. Huang, G. Yin, J. Zhang, Z. Zhang, P. Lai, B. Yan, Y. Chen, D. Jin, L. Wang, Characterization of a Novel Calcific Achilles Tendinopathy Model in Mice: Contralateral Tendinopathy Induced by Unilateral Tenotomy. *Calcified Tissue International*. **103**, 698–707 (2018).
50. N. S. Cho, J. H. Hwang, Y. T. Lee, S. W. Chae, Tendinosis-like histologic and molecular changes of the Achilles tendon to repetitive stress: a pilot study in rats. *Clinical Orthopaedics and Related Research*. **469**, 3172–3180 (2011).
51. J. Pingel, J. Wienecke, M. Kongsgaard, H. Behzad, T. Abraham, H. Langberg, A. Scott, Increased mast cell numbers in a calcaneal tendon overuse model. *Scandinavian Journal of Medicine & Science in Sports*. **23**, e353-360 (2013).
52. M. I. Almeida-Silveira, D. Lambertz, C. Pérot, F. Goubel, Changes in stiffness induced by hindlimb suspension in rat Achilles tendon. *European Journal of Applied Physiology*. **81**, 252–257 (2000).

53. Y. X. Liu, S. Thomopoulos, V. Birman, J.-S. Li, G. M. Genin, Bi-material attachment through a compliant interfacial system at the tendon-to-bone insertion site. *Mechanics of Materials: An International Journal*. **44** (2012), doi:10.1016/j.mechmat.2011.08.005.
54. G. M. Genin, A. Kent, V. Birman, B. Wopenka, J. D. Pasteris, P. J. Marquez, S. Thomopoulos, Functional Grading of Mineral and Collagen in the Attachment of Tendon to Bone. *Biophysical Journal*. **97**, 976–985 (2009).
55. J. Zhang, J. H.-C. Wang, Moderate Exercise Mitigates the Detrimental Effects of Aging on Tendon Stem Cells. *PloS One*. **10**, e0130454 (2015).
56. R. B. Svensson, K. M. Heinemeier, C. Couppé, M. Kjaer, S. P. Magnusson, Effect of aging and exercise on the tendon. *Journal of Applied Physiology*. **121**, 1353–1362 (2016).
57. Y. Sugiyama, K. Naito, K. Goto, Y. Kojima, A. Furuhata, M. Igarashi, I. Nagaoka, K. Kaneko, Effect of aging on the tendon structure and tendon-associated gene expression in mouse foot flexor tendon. *Biomedical Reports*. **10**, 238–244 (2019).
58. M. Franchi, A. Trirè, M. Quaranta, E. Orsini, V. Ottani, Collagen Structure of Tendon Relates to Function. *The Scientific World Journal*. **7**, 404–420 (2007).
59. X. Wang, R. A. Bank, J. M. TeKoppele, C. M. Agrawal, The role of collagen in determining bone mechanical properties. *Journal of Orthopaedic Research: Official Publication of the Orthopaedic Research Society*. **19**, 1021–1026 (2001).
60. P. Sharma, N. Maffulli, Tendon Injury and Tendinopathy: Healing and Repair. *JBJS*. **87**, 187 (2005).
61. S. E. Szczesny, C. Aeppli, A. David, R. L. Mauck, Fatigue Loading of Tendon Results in Collagen Kinking and Denaturation but Does Not Change Local Tissue Mechanics. *Journal of biomechanics*. **71**, 251–256 (2018).
62. M. Chatterjee, P. M. Muljadi, N. Andarawis-Puri, The role of the tendon ECM in mechanotransduction: disruption and repair following overuse. *Connective Tissue Research*. **63**, 28–42 (2022).
63. T. M. Ritty, R. Roth, J. E. Heuser, Tendon Cell Array Isolation Reveals a Previously Unknown Fibrillin-2-Containing Macromolecular Assembly. *Structure*. **11**, 1179–1188 (2003).
64. S. P. Arnoczky, M. Lavagnino, M. Egerbacher, The mechanobiological aetiopathogenesis of tendinopathy: is it the over-stimulation or the under-stimulation of tendon cells?:

Mechanobiological aetiology of tendinopathy. *International Journal of Experimental Pathology*. **88**, 217–226 (2007).

65. H. B. Sun, N. Andarawis-Puri, Y. Li, D. T. Fung, J. Y. Lee, V. M. Wang, J. Basta-Pljakic, D. J. Leong, J. B. Sereysky, S. J. Ros, R. A. Klug, J. Braman, M. B. Schaffler, K. J. Jepsen, E. L. Flatow, Cycle-dependent matrix remodeling gene expression response in fatigue-loaded rat patellar tendons. *J. Orthop. Res.* **28**, 1380–1386 (2010).

66. J. B. Holt, J. M. Pedowitz, P. H. Stearns, T. P. Bastrom, M. M. Dennis, J. R. Dwek, A. T. Pennock, Progressive Elbow Magnetic Resonance Imaging Abnormalities in Little League Baseball Players Are Common: A 3-Year Longitudinal Evaluation. *The American Journal of Sports Medicine*. **48**, 466–472 (2020).

67. A. T. Pennock, J. Dwek, E. Levy, P. Stearns, J. Manning, M. M. Dennis, A. Davis-Juarez, T. Bastrom, K. S. Taylor, Shoulder MRI Abnormalities in Asymptomatic Little League Baseball Players. *Orthopaedic Journal of Sports Medicine*. **6**, 2325967118756825 (2018).

68. A. G. Berman, J. M. Organ, M. R. Allen, J. M. Wallace, Muscle contraction induces osteogenic levels of cortical bone strain despite muscle weakness in a mouse model of Osteogenesis Imperfecta. *Bone*. **132**, 115061 (2020).

69. H. Leblond, M. L'Espérance, D. Orsal, S. Rossignol, Treadmill Locomotion in the Intact and Spinal Mouse. *Journal of Neuroscience*. **23**, 11411–11419 (2003).

70. K. G. Pearson, H. Acharya, K. Fouad, A new electrode configuration for recording electromyographic activity in behaving mice. *Journal of Neuroscience Methods*. **148**, 36–42 (2005).

71. L. K. Ritter, M. C. Tresch, C. J. Heckman, M. Manuel, V. M. Tysseling, Characterization of motor units in behaving adult mice shows a wide primary range. *Journal of Neurophysiology*. **112**, 543–551 (2014).

72. S. V. Brooks, J. A. Faulkner, Contractile properties of skeletal muscles from young, adult and aged mice. *The Journal of Physiology*. **404**, 71–82 (1988).

73. I. Kurtaliaj, M. Golman, A. C. Abraham, S. Thomopoulos, Biomechanical Testing of Murine Tendons. *Journal of visualized experiments : JoVE* (2019), doi:10.3791/60280.

74. M. I. Love, W. Huber, S. Anders, Moderated estimation of fold change and dispersion for RNA-seq data with DESeq2. *Genome Biology*. **15**, 550 (2014).

75. M. Stephens, False discovery rates: a new deal. *Biostatistics*. **18**, 275–294 (2017).

76. S. Anders, W. Huber, Differential expression analysis for sequence count data. *Genome Biology*. **11**, R106 (2010).
77. D. W. Huang, B. T. Sherman, R. A. Lempicki, Systematic and integrative analysis of large gene lists using DAVID bioinformatics resources. *Nat Protoc*. **4**, 44–57 (2009).
78. D. W. Huang, B. T. Sherman, R. A. Lempicki, Bioinformatics enrichment tools: paths toward the comprehensive functional analysis of large gene lists. *Nucleic Acids Research*. **37**, 1–13 (2009).

Acknowledgements
We thank the Advanced Genomics Core at the University of Michigan for library preparation and next-generation sequencing. We also thank Carol S. Davis and Susan V. Brooks for the support they provided for in vitro muscle contractility measurements. Schematics were made using Biorender.

Supplementary material: Table of content

Fig. S1	Fig. S1. Morphological comparisons, from histology and microcomputed tomography, of 5min loading bouts compared to 20min loading bouts.
Table S1	Descriptive statistics (Mean ± SD) and p-values from paired comparisons (two-tailed) of bone morphometric measurements of the posterior calcaneus in the 5-minute loaded samples compared to contralateral controls
Fig. S2	Quantitative real-time reverse transcription polymerase chain reaction (qRTPCR) validation of results from bulk RNA-sequencing (tendon)
Supplemental material S3	"adf4683_Suppl. Excel_seq1_v1.xlsx": List of differentially expressed genes in tendon and bone

Funding
This work was supported by the National Institutes of Health (NIAMS-R01AR079367, NIBIB-U24EB029011, NIAMS-R01AR076120, NHLBI-R01HL135568, NIBIB-R01EB016701, NIGMS-P41GM103545, NIGMS-P30GM103333, NICHD-R03HD094594, and NIAMS-P30AR069620), the National Science Foundation (NSF CAREER #1944448), the Michigan-

Israel Partnership for Research and Education, and the Beckman Institute for Advanced Science and Technology.

Author Contributions

Conceptualization: EG, SNL, MS, NW, ACA, MLK

Methodology: EG, SNL, ACA, MLK

Investigation: EG, SNL, RWG

Visualization: EG, SNL, MLK

Supervision: MLK

Writing—original draft: EG, SNL, MS, NW, ACA, MLK

Writing—review & editing: EG, SNL, MS, NW, RWG, ACA, MLK

Competing Interests

All authors declare they have no competing interests.